E S O   S c i e n c e   A r c h i v e   F a c i l i t y   -   P h a s e   3   D a t a   R e l e a s e   D e s c r i p t i o n
ESO public survey programme VINROUGE - VIsta Near-infraRed Observations Unveiling Gravitational wave Events, Data Release DR1
provided by Nial Tanvir, submitted on 2019-08-08, published on 2019-08-09

# VINROUGE – VIsta Near infra-Red Observations Uncovering Gravitational wave Events


## Abstract

The data released here were obtained with the VIRCAM instrument on VISTA under programme 198.D-2010. They consist of Y, J & Ks band imaging, and their associated object catalogues, of portions of the error regions for gravitational wave events found during the second LIGO/Virgo science run, O2. Specifically, the events triggered on were the binary black hole mergers GW170809 (~17 sq-deg), GW170814 (~27 sq-deg) and the binary neutron star merger GW170817 (~3.5 sq-deg). For the latter case, the kilonova counterpart of the merger was identified in the second field observed on the first night, and thereafter this field was re-observed for 14 further epochs over the subsequent ~3 weeks.


## Overview of Observations

The primary goals of the VINROUGE survey are to locate and characterize the electromagnetic counterparts of gravitational wave discovered events. This is achieved through wide field, multi-filter imaging of the error regions with VIRCAM on VISTA. This data-release contains imaging and catalogues obtained during the follow-up of three gravitational wave triggers during the second LIGO/Virgo science run (O2). Coincidently, the three events occurred within a few days of each other, culminating the first binary neutron star detection. This rapid series of triggers of increasing importance meant that the initially planned follow-up of the earlier events was curtailed. Further specifics of the three campaigns are as follows:

**GW170809** (trigger G296853) was a binary black hole event detected on 9th Aug 2017. The initial 90% error region covered an area of 1160 sq-deg. The ultimately published analysis (Abbott et al. 2019) estimated a luminosity distance was 980 Mpc and 90% error region on the sky of 310 sq-deg. Our observations in the YJKs filters took place on UT date 14th Aug 2017 and covered an area of approximately 17 sq-deg, overlapping with existing imaging from the VIKING Survey and was around the peak of the GW likelihood (see Fig. 1). Although 14 tiles were originally planned, two were not observed due to the trigger being curtailed by the advent of GW170814.

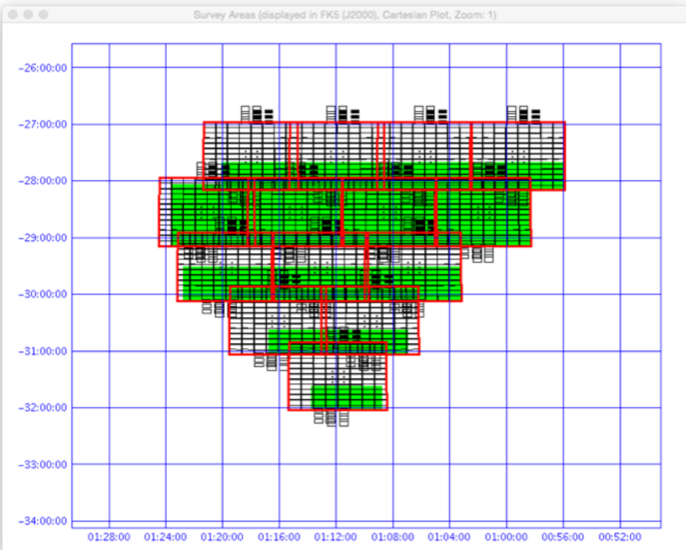


***Fig. 1*** *Locations of the tiles requested for observation in the follow-up of GW170809. Note, the two tiles at dec=-30.5 deg were planned but ultimately not observed.*

**GW170814** (trigger G297595) was a binary black hole event detected on 14th Aug 2017 and was the first to benefit from significant improvement in the location error region due to the combination of data from all three detectors (LIGO-Hanford, LIGO-Livingston and Virgo). The initial 90% error region covered an area of 97 sq-deg. The ultimately published analysis (Abbott et al. 2019) estimated a luminosity distance was 570 Mpc and 90% error region on the sky of 87 sq-deg. Our observations in the YJKs filters took place on UT date 15th and 16th Aug 2017, although the error region was updated between these epochs, which resulted in a significant movement on the sky (in RA) rendering the first epoch observations (15 tiles covering approx. 18 sq-deg) no longer in the high likelihood region. The sky area covered in the observations made on the 16th was approximately 9 sq-deg (7 tiles), and is shown in Fig. 2.

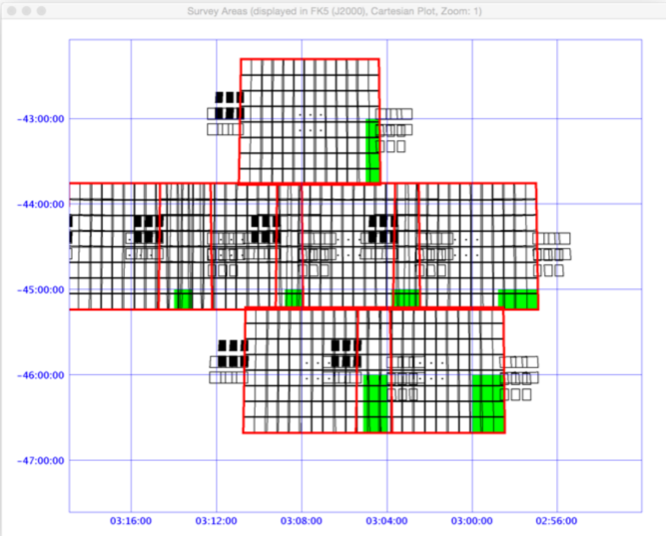


***Fig. 2*** *Locations of the tiles observed in the follow-up of GW170814 based on the revised error region (the first observations following-up this event used the original error region which is displaced earlier in RA and outside the revised high-likelihood region).*

**GW170817** (trigger G298048) was a binary neutron star event detected on 17th Aug 2017. The initial trigger was based on information from only one LIGO detector, and so provided a very poor localization. However, within a few hours an updated three detector localization was achieved with an error region of only 31 sq-deg (ultimately refined to 16 sq-deg; Abbott et al. 2019), together with an estimated distance of 40 Mpc. Our observations began in twilight on the 17th, and consisted of Y,J,Ks imaging of two tiles selected to contain a high density of galaxies with high likelihood of being the host (Fig. 3). The kilonova counterpart was imaged in the second of these fields (Abbott et al. 2017). Second epoch observations were gathered immediately after the first epoch was finished. Further imaging of the field containing the counterpart was obtained over the next 3 weeks as the kilonova faded (later observations were only obtained in the Ks band), and the field was still accessible in the early part of the night (Tanvir et al. 2017).

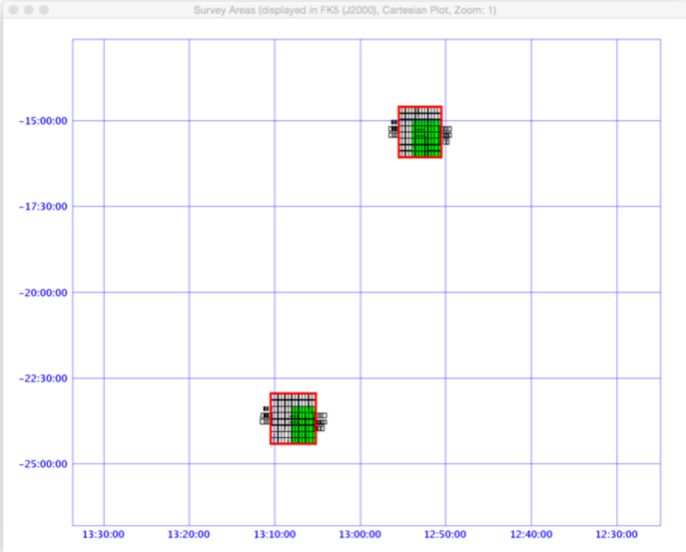


***Fig. 3*** *Locations of the two tiles observed during the first epoch of observations of GW170817. The more southerly field was found to contain the counterpart, and this field was re-observed at further epochs.*

## Release Content

All observations consist of imaging, confidence maps and associated object catalogues. In the majority of cases full tiles were observed (exceptions are noted), but in any case, individual paw-print images are also in the release. Since the observations were time-critical and made with the particular objective of discovering possible counterparts to GW events, and, in the case of GW170817, monitoring the kilonova found, the depths and imaging quality achieved depend on the conditions on the night and exposure times used, and are therefore not uniform.

Typical limiting AB magnitudes per tile are Y=21.0, J=21.0, K=20.1. The total number of multi-extension fits image files is 883 corresponding to 60.5 GB. The total volume of catalogue data is 5.1 GB.

**GW170809**

The following tile centres were observed, in each case with Y,J,Ks bands and total exposure time per tile per band of 6 mins (i.e. 1 min per paw-print):

```
00 59 13.20 -27 33 59.0
01 05 46.63 -27 33 59.0
01 11 57.48 -27 33 59.0
01 18 00.84 -27 33 59.0
01 01 37.92 -28 32 58.9
01 08 14.90 -28 32 58.9
01 14 51.89 -28 32 58.9
01 21 06.10 -28 32 58.9
01 06 33.38 -29 31 14.2
01 13 06.38 -29 31 14.2
01 19 47.06 -29 31 14.2
01 11 53.04 -31 26 58.2
```

**GW170814**

The following tile centres were observed, in each case with Y,J,Ks bands and total exposure time per tile per band of 6 mins (i.e. 1 min per paw-print):

*Night 1*

```
02 39 11.95 -44 30 09.4
02 35 50.59 -45 57 04.3
02 35 09.79 -47 24 34.6
02 47 55.10 -43 02 47.4
02 35 21.98 -48 52 04.4
02 51 55.70 -41 34 36.5
02 39 47.86 -47 24 33.5
02 41 10.18 -45 57 07.6
02 45 02.18 -45 57 08.3
02 44 41.98 -44 30 12.2
02 49 53.98 -44 30 12.2
02 52 58.87 -43 02 39.5
02 54 49.61 -41 34 37.6
02 50 40.18 -45 57 03.2
02 44 05.45 -47 24 37.4
```

*Night 2*

```
03 05 48.96 -44 30 11.5
03 11 18.96 -44 30 11.5
03 00 17.98 -44 30 12.2
03 07 36.77 -43 02 43.4
03 01 56.45 -45 57 05.4
03 07 14.93 -45 57 06.5
03 15 35.28 -44 30 12.2
```

**GW170817**

*First night observations:*
The following tile centres were observed twice on the first night, in each case with Y,J,Ks bands obtained at the first visit, and respectively J, Ks for the southerly field and just Ks for the northerly field at the second visit. The total exposure time per tile per band was 6 mins (i.e. 1 min per paw-print):

```
13 07 47.33 -23 41 48.5
12 52 59.33 -15 20 43.4
```

*Further monitoring:*
Subsequent epochs were obtained only of the kilonova location, with filter selection depending on the available time and evolving kilonova luminosity. Specifically, the refined tile centre used was:

```
13 08 37.15 -23 35 48.5
```

Start time details of the individual tile exposures for the kilonova field are given below, with notes including an estimate of the on-frame seeing:

*Y epochs*

```
2017-08-18 00:15:34.7  1.15”
2017-08-18 23:53:25.3  1.07”
2017-08-19 23:48:57.6  1.81”
2017-08-20 23:44:33.0  1.00”
2017-08-21 23:42:31.6  1.07”
2017-08-23 23:59:51.8  1.13”
2017-08-24 23:47:44.6  0.97”
2017-08-25 23:36:05.4  0.82”   Single paw-print, 4x60s
2017-08-26 23:38:35.2  0.98”
```

*J epochs*

```
2017-08-18 00:06:11.6  1.15”
2017-08-18 00:49:29.1  1.45”
```

```
2017-08-18 23:44:06.3  0.94”
2017-08-19 23:39:13.6  1.42”
2017-08-20 23:33:58.4  0.95”
2017-08-21 23:33:16.3  0.95”
2017-08-23 23:50:28.0  1.05”
2017-08-24 23:37:28.7  0.90”
2017-08-25 23:30:31.5  0.74”   Single paw-print, 4x60s
2017-08-26 23:28:55.2  0.86”
2017-08-27 23:32:07.2  0.99”
2017-08-28 23:23:56.8  1.15”
2017-08-28 23:33:36.5  1.13”
2017-08-28 23:43:09.2  1.21”
```

*Ks epochs*

```
2017-08-17 23:55:40.2  1.06”
2017-08-18 00:39:37.2  1.07”
2017-08-18 23:34:21.4  0.87”
2017-08-19 23:29:23.0  1.24”
2017-08-20 23:24:06.6  0.87”
2017-08-21 23:23:26.9  0.93”
2017-08-23 23:40:29.1  0.89”
2017-08-24 23:27:30.9  0.88”
2017-08-25 23:24:44.7  0.77”   Single paw-print, 4x60s
2017-08-26 23:19:00.8  0.97”
2017-08-27 23:22:08.7  0.89”
2017-08-27 23:41:47.4  0.98”
2017-08-29 23:29:10.1  1.34”
2017-08-29 23:39:40.8  1.18”
2017-08-31 23:31:23.5  0.90”
2017-08-31 23:42:35.1  1.05”
2017-09-06 23:29:37.3  0.90”
```

# Release Notes

Imaging processed through the standard VDFS pipeline.

## Data Reduction and Calibration

This data release is based on the CASU version v1.5 pipeline. Full details of the data pipeline procedure and the version changes can be found at: http://casu.ast.cam.ac.uk/surveys-projects/vista

The photometric and astrometric calibrations are both derived from the 2MASS Point Source Catalogue. The photometric calibration includes an additional colour term designed to correct for the effect of interstellar extinction on the 2MASS to VISTA/VIRCAM photometric transformations. Magnitudes are in a Vega-like system, and absolute zero point offsets and AB transformation, including illumination correction, can be found in Gonzalez Fernandez et al. (2018).

The CASU pipeline derives aperture photometry for all detected sources on each image. Detection criteria require potential sources to have 4 adjacent pixels that are above 1.25 times the local background dispersion. Magnitudes are aperture-corrected using a curve-of-growth method, and in the case of mosaic images, each source has had a correction applied that compensates the seeing variation in the individual pawprint images that make the mosaic. This process is known as grouting, and more detail can be found in Gonzalez Fernandez et al. (2018).

The photometric catalogues contain calibrated aperture photometry, the limiting magnitudes that correspond to the aperture photometry and the saturation limit for the point sources.

No correction has been made for the effects of extinction.

## Data Quality

Detailed information about pipeline performance can be found in Gonzalez Fernandez et al. (2018). Photometric consistency in J and Ks is of 2% for the linear dynamic range of the instrument. Astrometric errors are of around 50 mas for stacked pawprints.

No systematic errors are detected at these levels, either in astrometry or photometry, except for known issues detailed in the next section.

Stacked pawprints are visually inspected both for stacking errors and variations in sky background.

## Known issues

There are a number of well known image defects intrinsic to VISTA, e.g. holes in some of the arrays and bright streaks caused by reflections of stars located just off the edge of an array. These defects are documented in Sutherland et al. 2015 (Sutherland et al. 2015), and they are illustrated with pictures in the CASU web page located at: http://casu.ast.cam.ac.uk/surveys-projects/vista/technical/known-issues

# Data Format

## Files Types

There are 6 types of file, all in FITS format. Pawprint images (file names ending in "_st.fits.fz"), associated weight maps (file names ending in "_st_conf.fits.fz") and pawprint catalogues (file names ending in "_st_cat.fits"). Tile images (file names ending in "_st_tl.fits.fz"), associated weight maps (file names ending in "_st_tl_conf.fits.fz") and tile catalogues (file names ending in "_st_tl_cat.fits").

## Catalogue Columns

More information is available at
http://casu.ast.cam.ac.uk/surveys-projects/vista/technical/catalogue-generation

| No. | Name | Column Description |
|---|---|---|
| 1 | Seq No. | running number for ease of reference, in strict order of image detections |
| 2 | Isophotal flux | standard definition of summed flux within detection isophote, apart from detection filter is used to define pixel connectivity and hence which pixels to include. This helps to reduce edge effects for all isophotally derived parameters. |
| 3 | X coord | intensity–weighted isophotal centre–of–gravity in X |
| 4 | Error in X | estimate of centroid error |
| 5 | Y coord | intensity–weighted isophotal centre–of–gravity in Y |
| 6 | Error in Y | estimate of centroid error |
| 7 | Gaussian sigma | these are derived from the three general intensity–weighted second moments |
| 8 | Ellipticity | the equivalence between them and a generalised elliptical Gaussian |
| 9 | Position angle | |
| 10 | Areal profile 1 | number of pixels above a series of threshold levels relative to local sky. |

| | | |
|---|---|---|
| 11 | Areal profile 2 | levels are set at T, 2T, 4T, 8T . . . 128T where T is the threshold. These |
| 12 | Areal profile 3 | can be thought of as a sort of poor man's radial profile. Note that for now |
| 13 | Areal profile 4 | deblended, i.e. overlapping images, only the first areal profile is computed |
| 14 | Areal profile 5 | and the rest are set to −1 flagging the difficulty of computing accurate |
| 15 | Areal profile 6 | profiles |
| 16 | Areal profile 7 | |
| 17 | Areal profile 8 | for blended images this parameter is used to flag the start of the sequence of the deblended components by setting the first in the sequence to 0 |
| 18 | Peak height | in counts relative to local value of sky - also zeroth order aperture flux |
| 19 | Error in pkht | |
| 20 | Aperture flux 1 | These are a series of different radii soft-edged apertures designed to adequately sample the curve-of-growth of the majority of images and to provide fixed-sized aperture fluxes for all images. The scale size for these apertures is selected by defining a scale radius <FWHM> for site+instrument. In the case of VIRCAM this "core" radius (rcore) has been fixed at 1.0 arcsec for convenience in inter-comparison with other datasets. A 1.0 arcsec radius is equivalent to 3.0 pixels for normal data. In 0.8 arcsec seeing an rcore-radius aperture contains roughly 75% of the total flux of stellar images. [In general the rcore parameter is user specifiable and hence is recorded in the output catalogue FITS header.]<br>The aperture fluxes are sky-corrected integrals (summations) with a soft-edge (ie. pro-rata flux division for boundary pixels). However, for overlapping images they are more subtle than this since they are in practice simultaneously fitted top-hat functions, to minimise the effects of crowding. Images external to the blend are also flagged and not included in the large radius summations. |
| 21 | Error in flux | |
| 22 | Aperture flux 2 | |
| 23 | Error in flux | |
| 24 | Aperture flux 3 | Recommended if a single number is required to represent the flux for ALL |
| 25 | Error in flux | images - this aperture has a radius of rcore. |
| 26 | Aperture flux 4 | |
| 27 | Error in flux | Starting with parameter 20 the radii are:<br>1/2× rcore, 1/sqrt(2)× rcore, rcore, sqrt(2)× rcore, 2× rcore, 2sqrt(2)× rcore, 4× rcore, 5× rcore, 6× rcore, 7× rcore, |
| 28 | Aperture flux 5 | 8× rcore, 10× rcore, 12× rcore |

| | | |
|---|---|---|
| 29 | Error in flux | |
| 30 | Aperture flux 6 | Note 4× rcore, ensures ∼ 99% of PSF flux |
| 31 | Error in flux | |
| 32 | Aperture flux 7 | extras for generalised galaxy photometry further spaced |
| 33 | Error in flux | |
| 34 | Aperture flux 8 | in radius to ensure reasonable sampling further out. |
| 35 | Error in flux | |
| 36 | Aperture flux 9 | |
| 37 | Error in flux | |
| 38 | Aperture flux 10 | Note these are all corrected for pixels from overlapping neighbouring images |
| 39 | Error in flux | |
| 40 | Aperture flux 11 | |
| 41 | Error in flux | |
| 42 | Aperture flux 12 | |
| 43 | Error in flux | |
| 44 | Aperture flux 13 | The biggest with radius 12× rcore ie. about 24 arcsec diameter |
| 45 | Error in flux | The aperture fluxes can be combined with later-derived aperture corrections for general purpose photometry and together with parameter 18 (the peak flux) give a simple curve–of–growth measurement which forms the basis of the morphological classification scheme |
| 46 | Petrosian radius | rp as defined in Yasuda et al. 2001 AJ 112 1104 |
| 47 | Kron radius | rk as defined in Bertin and Arnouts 1996 A&A Supp 117 393 |
| 48 | Half-light radius | rh estimate of half-light radius |
| 49 | Petrosian flux | flux within circular aperture to k x rp with k=2 |
| 50 | Error in flux | |
| 51 | Kron flux | flux within circular aperture to k x rk with k=2 |

| | | |
|---|---|---|
| 52 | Error in flux | |
| 53 | Half-light flux | flux within circular aperture to k x rh with k=1 |
| 54 | Error in flux | |
| 55 | Error bit flag | bit pattern listing various processing error flags<br>initially set to the no. of bad pixels within aperture of radius "rcore"<br>- note this can be fractional due to soft-edged apertures |
| 56 | Sky level | local interpolated sky level from background tracker |
| 57 | Sky rms | local estimate of variation in sky level around image |
| 58 | Av conf | average confidence level within default rcore aperture<br>useful for spotting spurious outliers in various parameter selection spaces |
| | | The following are accreted after standard catalog generation |
| 59 | RA | RA and Dec explicitly put in columns for overlay programs that cannot, |
| 60 | Dec | in general, understand astrometric solution coefficients – note r*4<br>storage precision accurate only to ~ 50mas. Astrometry can<br>be derived more precisely from WCS in header and XY in parameters 5 & 6 |
| 61 | Classifica-tion | Flag indicating most probable morphological classification:<br>eg. –1 stellar, +1 non–stellar, 0 noise, –2 borderline stellar<br>(Saturated images can be flagged by comparing the peak height + local<br>sky with the SATURATE keyword in the header.) |
| 62 | Statistic | An equivalent N(0,1) measure of how stellar–like an image is, used in<br>deriving parameter 61 in a 'necessary but not sufficient' sense.<br>Derived mainly from the curve-of-growth of flux using the well-defined<br>stellar locus as a function of magnitude as a benchmark<br>(see Irwin et al. 1994 SPIE 5493 411 for more details). |
| 63 | MJDOff | For tile catalogues only this column represents the median MJD offset of the object with respect to the MJD of the day of observation (recorded in the header as MJD_DAY). |
| 64 | Blank64 | |
| 65 | Blank65 | |
| 66 | Blank66 | |
| 67 | Blank67 | |
| 68 | Blank68 | |
| 69 | Blank69 | |
| 70 | Blank70 | |
| 71 | Blank71 | |
| 72 | Blank72 | |
| 73 | Blank73 | |
| 74 | Blank74 | |
| 75 | Blank75 | |

| | | |
|---|---|---|
| 76 | Blank76 | |
| 77 | Blank77 | |
| 78 | Blank78 | |
| 79 | Blank79 | |
| 80 | Blank80 | |


## Acknowledgements

*Any publication making use of this data, whether obtained from the ESO archive or via third parties, must include the following acknowledgment:*

- "Based on data products created from observations collected at the European Organisation for Astronomical Research in the Southern Hemisphere under ESO programme(s) 198.D-2010(A)"

*If access to the ESO Science Archive Facility services was helpful for your research, please include the following acknowledgment:*

- "This research has made use of the services of the ESO Science Archive Facility."



*Science data products from the ESO archive may be distributed by third parties, and disseminated via other services, according to the terms of the [Creative Commons Attribution 4.0 International license](). Credit to the ESO origin of the data must be acknowledged, and the file headers preserved.*


## References


Abbott, B. P. et al. 2017 ApJ 848 L12
Abbott, B. P. et al. 2019 ApJ 875 161
Gonzalez Fernandez, C. et al. 2018 MNRAS 474 5459
Sutherland et al. 2015, A&A, 575, A25
Tanvir, N. R. et al. 2017 ApJ 848 L27